Resonance Issues and Damping Techniques for Grid-Connected Inverters With Long Transmission Cable

Shao Zhang, *Member, IEEE*, Shuai Jiang, *Student Member, IEEE*, Xi Lu, *Student Member, IEEE*, Baoming Ge, *Member, IEEE*, and Fang Zheng Peng, *Fellow, IEEE*

***Abstract*—An infinite source with series inductance is usually employed as a grid emulator in grid-connected distributed generation systems. Thus, high capacitance of a transmission cable (i.e., underground cable) is too significant to be neglected. As a result, the capacitance and inductance may cause system resonance, which, in turn, challenges system stability. This paper takes offshore wind farm as an example to investigate the resonance issues caused by the submarine transmission cable of the grid-connected generation system. Based on the submarine cable model, a series of considerable resonant peaks is found in the open-loop transfer function of the grid-connected system because of the high-order *LC* configuration. The resonant peaks are sensitive to the system setup, which is clearly investigated. To overcome the resonances, this paper proposes a cascaded notch-filter-based active damping method to guarantee a good system stability and robustness. Furthermore, the proposed controller employs a proportional-resonant component to reduce the steady-state error of the output current. The simulation and experimental results have validated the findings of resonances and the effectiveness of the proposed controller.**

***Index Terms*—Frequency analysis, resonant damping, transmission cable, voltage source inverter (VSI), wind turbine.**

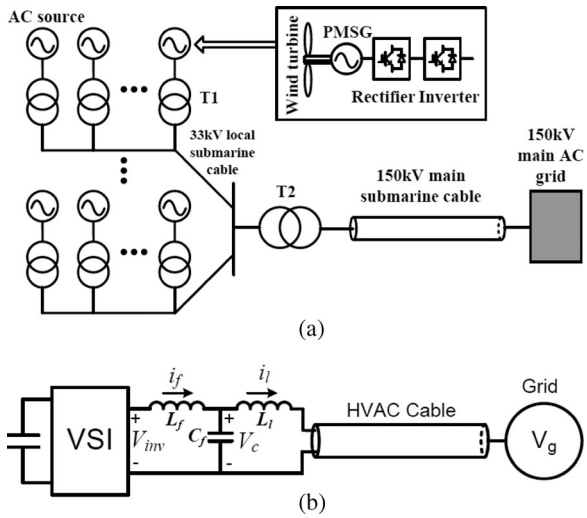

Fig. 1. Typical offshore wind generation system with an HVac transmission cable. (a) System configuration. (b) Equivalent circuit.

I. Introduction

A POWER electronic converter plays an important role in distributed generation and in integration of renewable energy sources into an electrical grid [1], [2]. Taking modern wind turbine as an example, it often adapts back-to-back voltage source inverter (VSI) for grid connection via either high-voltage ac (HVac) or HVdc transmission cable [3], [4]. Among the existing offshore wind farms, the HVac interconnection has been widely used, such as in Denmark's Horns Rev wind farm, Nysted wind farm, United Kingdom's Barrow wind farm, and so on [5]. Fig. 1(a) shows the configuration of a typical wind generation system with an HVac transmission cable. In practice, a group of wind generators are connected to an onshore point of common coupling (PCC) through VSI, step-up transformers, and HVac submarine cables [6].

Manuscript received November 2, 2012; revised January 10, 2013 and March 6, 2013; accepted March 7, 2013. Date of current version July 18, 2013. Recommended for publication by Associate Editor C. N. M. Ho.

The authors are with the Department of Electrical and Computer Engineering, Michigan State University, MI 48824 USA (e-mail: zhan0192@e.ntu.edu.sg; jiangshu@msu.edu; luxi1@msu.edu; gebm@msu.edu; fangzpeng@gmail.com).

Color versions of one or more of the figures in this paper are available online at http://ieeexplore.ieee.org.

Digital Object Identifier 10.1109/TPEL.2013.2253127

It is well known that the switching-mode power converter (i.e., VSI) would generate harmonics, which potentially pollute the connected utility. To prevent the pollution of the utility due to a high-frequency current ripple, a filter, typically *LC* type, is usually installed at the output of the inverter [7]–[9]. The capacitor is used to provide a low-impedance path for the high-frequency components. The equivalent circuit of the typical grid-connected wind generation system is shown in Fig. 1(b), in which L_l is the lumped inductance of the local cable inductance and the leakage inductances of the transformers T1 and T2. Conventionally, the transmission line is simplified as an inductor for the convenience of a grid-connected inverter design [10]–[12]. Hence, the inverter actually outputs with an equivalent *LCL* filter. Thus, systems incorporating *LCL* filters are of third order, and they require more complex current control strategies to maintain system stability, and are more susceptible to interference from grid voltage harmonics because of resonance hazards and the lower harmonic impedance presented to the grid [13]–[17].

Passive and active damping techniques are often used to attenuate the resonant peaks caused by the *LCL* filter. The popular passive damping is to insert a damping resistor in the capacitor shunt branch of the *LCL* filter [18], [19] or split the capacitor of the *LCL* filter into two parts [20]. However, the passive damping causes a decrease of the overall system efficiency because of the losses on the additional components. Alternatively,

multiloop- and filter-based active damping techniques were developed to eliminate the resonant peaks instead of adding any passive devices. In the multiloop-based damping, more system state variables are involved into the control loop to guarantee the system stability [7], [13], [21]–[27]. It means that two or even more control loops are required to damp the system resonant peaks. In the filter-based damping methods, a higher order controller (filter) is used to regulate the low-frequency dynamics and damp the potentially unstable high-frequency dynamics [28]–[32]. The design of the filter can be divided into analogy- and digital-based approaches. In both cases, this kind of active damping methods has the advantage that it does need fewer sensors [33].

As aforementioned, the transmission line is usually equivalent as the inductor. However, because of a relatively long distance from the inverter to the onshore main grid, the distributed inductance and capacitance along the HVac transmission system are too significant to be ignored [34], [35], for example, typically in the range of 100–150 kvar/km for 33-kV cross-linked polyethylene (XLPE) cables, 1000 kvar/km for 132-kV XLPE cables, and 6–8 Mvar/km for 400-kV XLPE cables [5]. Due to the high capacitance of the cable, a series of resonances may occur between the onshore and offshore grids, and leads to a distortion in the shape of the voltage/current [36], which, in turn, potentially results in system instability. To analyze the essential behavior of resonances, it is necessary to have the accurate calculation of the cable impedances, which were discussed in [37] and [38]. The modeling methodology for the main components (i.e., three-conductor cable and power transformers) of the wind power plant was developed for the investigation of transient performance [39].

This paper developed a per-unit scale single-phase equivalent model of the HVac-connected wind generation system. The system modeling is derived with consideration of the HVac cable characteristics, and frequency-domain analysis is provided for better understanding of system essential behavior. Due to the high-order *LC* configuration for a long-distance transmission cable, the system open-loop transfer function exhibits a series of significant high-frequency resonant peaks, which makes the control loop gain of a conventional controller quite small in order to guarantee system stability. Consequently, the steady-state error of the system output (i.e., current) is too significant and thereby the feedback is unable to track a sinusoidal reference. This paper proposes a cascaded notch-filter-based active damping method to eliminate the considerable resonant peaks. Furthermore, the proposed controller employs a proportional-resonant (PR) component to reduce the steady-state error of the output current. In order to facilitate the simulations and experimental tests, all per-unit parameters of a real transmission cable are proportionally reconstructed in the 120 V_{ac} experimental emulator system. The simulation and experimental results verify the disclosed resonance phenomena and the performance of the proposed controller.

II. System Modeling

Traditionally, the grid is emulated by the infinite source with the series inductance in grid-connected distributed generation systems. However, high capacitance of a transmission cable is too significant to be neglected, especially for submarine transmission cables. Hence, it is necessary to take into consideration the cable capacitance, which is discussed in the following paragraphs.

A. System Description

The European Horns Rev offshore wind farm has a capacity of 160 MW, which is connected to the shore through a 15-km-long three-core ac cable with a rated voltage of 150 kV. The United Kingdom's 90-MW Burbo wind farm is connected to the onshore grid through a 33-kV 12-km-long ac cable. The England's 367-MW Walney wind farm is also connected to an onshore grid through a 132-kV 40-km-long ac cable. In fact, HVac transmission is adopted by all existing wind farms [5]. As aforementioned, the HVac cables have considerable impedance, typically in the range of 100–150 kvar/km for 33-kV cross-linked polyethylene (XLPE) cables and 1000 kvar/km for 132-kV XLPE cables. Taking the 160 MW/150 kV Horns Rev offshore wind farm as an example, the capacitance and inductance of these HVac cables are up to 20% and 15%, respectively. In practice, flexible ac transmission system (FACTS) devices are often required to be installed for grid compliance of wind power penetration [40], [41]. However, the FACTS devices are normally quite expensive, especially for high power capacity. Instead of FACTS, the design of the front-end VSI is required to take count in the complete load characteristics, which is the combination of the filter, step-up transformers, and HVac cable, as illustrated in Fig. 1.

B. Conventional Approaches to Build a System Model

A wire is usually simplified as a lumped inductor for the design of VSI. The equivalent circuit of the typical offshore wind generation system is shown in Fig. 1(b). Herein, the *LC*-type filter is adapted because of its wide application in VSI, which aims to filter out all of the inverter output harmonics but the fundamental frequency. The VSI system consists of the *LC* filter, the lumped leakage inductance of the transformers, and the lumped inductance of the cable. The current flowing into cable I_l can be represented by the average output voltage of inverter $V_{\rm inv}$ and grid voltage V_g by

$$\begin{aligned} I_l(s) &= \frac{1}{s\left[L_f+L_l+L_{\rm cable}+\left(L_l+L_{\rm cable}\right)L_fC_fs^2\right]}\cdot V_{\rm inv}(s) \\ &\quad+\frac{-L_fC_fs^2-1}{s\left[L_f+L_l+L_{\rm cable}+\left(L_l+L_{\rm cable}\right)L_fC_fs^2\right]}\cdot V_g(s) \\ &= G^{\rm old}_{V_{\rm inv}\to I_l}(s)\cdot V_{\rm inv}(s)+G^{\rm old}_{V_g\to I_l}(s)\cdot V_g(s) \end{aligned} \tag{1}$$

where $L_{\rm cable}$ and L_l are the lumped inductance of the transmission cable and the lumped leakage inductance of the step-up transformers, respectively. L_f and C_f are the filter inductance and capacitance, respectively. $G^{\rm old}_{V_{\rm inv}\to I_l}$ and $G^{\rm old}_{V_g\to I_l}(s)$ are the transfer functions from the current I_l to the inverter output voltage $V_{\rm inv}$ and the grid voltage V_g, respectively.

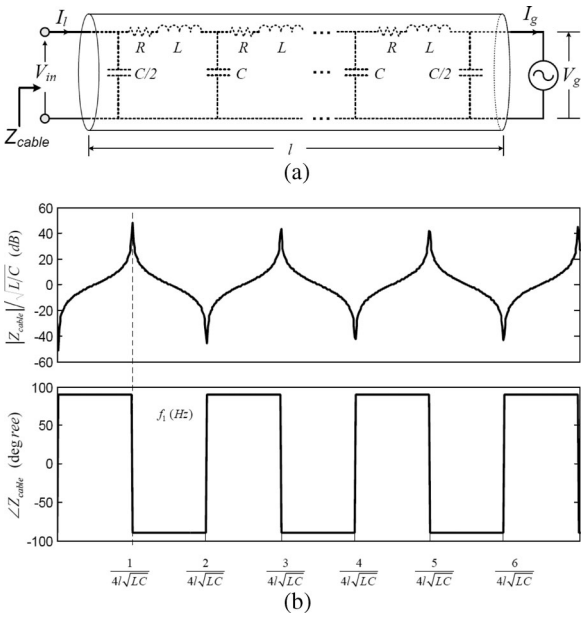

Fig. 2. One phase of an HVac cable. (a) Schematic diagram. (b) Impedance of a cable of length l terminated in a short circuit.

The control aim is to make the current I_l track with the reference, which, in turn, delivers renewable (wind) power into the grid. However, the whole systems are of third order, and they require more complex current control strategies to prevent resonance phenomenon. To damp the resonance, the solutions mainly include two types: passive damping methods and active (multiloop- or filter-based) damping methods, which has been discussed previously.

C. Proposed System Model

1) Characteristic of a Real Transmission Cable: Fig. 2 shows the schematic diagram of one-phase HVac cable as well as its impedance characteristic. As shown in Fig. 2(a), the input impedance of a lossless transmission cable terminated with an ideal voltage source is defined as [35]

$$Z_{\text{cable}} = \frac{V_{\text{in}}}{I_L} = Z_C \frac{Z_g/Z_C + \tanh(\gamma l)}{(Z_g/Z_C)\tanh(\gamma l) + 1} \tag{2}$$

where $Z_g = V_g/I_g$ is the grid-side impedance, $\gamma = \sqrt{z \cdot y}$ is the propagation constant, and $Z_C = \sqrt{z/y}$ is the characteristic impedance of the line. For a lossless transmission cable, $z = j\omega L$ and $y = j\omega C$ are the series impedance and shunt admittance of the cable in per-unit length, respectively. From (2), Z_{cable} of the lossless transmission line is a transcendental function with an infinite number of j-axis poles and zeros. Fig. 2(b) shows the theoretical Z_{cable} of the transmission cable, when Z_g is zero.

On the other hand, it is worthy to point out that the current density in ac circuits is greater near the outer surface of the conductor, which is the so-called skin effect. Near to the center of the conductor, there are more lines of magnetic force than near the rim. This causes an increment in the inductance toward the center and the current tends to crowd toward the outer surface. As a consequence, with the increase of operating frequencies, the effective cross-sectional area of the conductor would decrease and thereby the ESR along the cable becomes dominant, giving sufficient passive damping naturally [42]. Considering the skin effect in a cylindrical conductor, the ESR along the cable can be expressed in the Laplace form as

$$R_{\text{ESR}}(s) = R_0 \frac{1}{1 - \left(1 - \sqrt{\frac{j2\pi f_0}{s}}\right)^2} \tag{3}$$

where R_0 is the ESR at f_0. The parameters are listed in Table I. Hence, with the skin effect, the poles and zeros of the conductor could be attenuated accordingly when the frequency increases. Fig. 3 shows the admittance characteristic of a transmission cable with the skin effect. The cable parameters used here are listed in Table I.

2) System Model With Cable Characteristic: According to the cable characteristic, the capacitance can no longer be ignored during the system design. In other words, lumped inductance-based method is not accurate enough to model the submarine cable for transient analysis due to the considerable distributed capacitance along the cable. Hence, the cascaded π-segments are adapted to model the cable for exploring the system dynamic performance [43]. With the cable impedance in (2), (1) can be

TABLE I
SYSTEM PARAMETERS

System ratings	Value (SI)
Rated power	960 W
Grid voltage V_g	120 V / 60 Hz
Cable model parameters	
Number of π-cells	6
Cable inductance per cell (L)	0.6 mH
Cable capacitance per cell (C)	3 μF
ESR per cell (r_0) @ 20 Hz	72.5 mΩ
Inverter parameters	
Switching frequency	10 kHz
DC-link voltage	200 V
Filter inductance (L_f)	0.6 mH
Filter capacitance (C_f)	15 μF
Transformer Leakage inductance (L_l)	0.6 mH

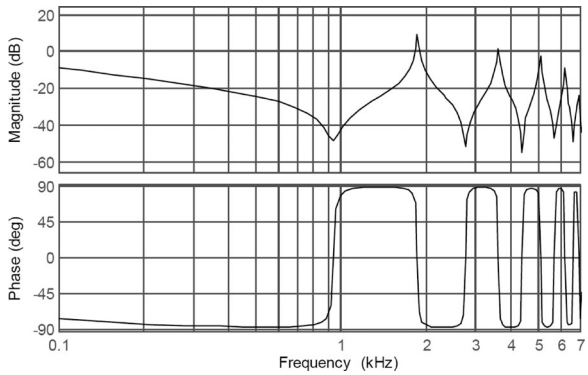

Fig. 3. Admittance characteristic of the transmission cable.

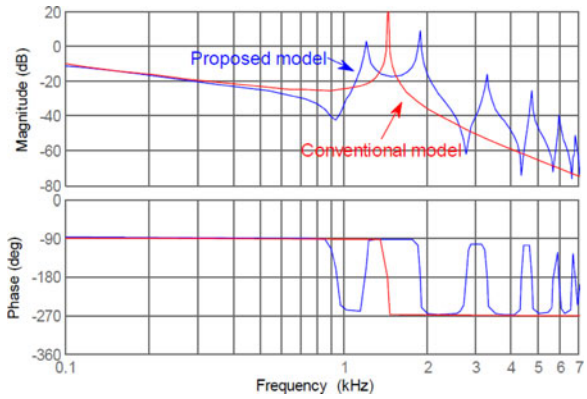

Fig. 4. Bode diagrams of $G_{V_{\rm inv}\to I_l}(s)$ from the conventional and proposed model.

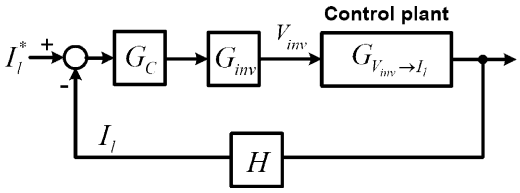

Fig. 5. Conventional current control for a grid-connected inverter.

updated as

$$I_l(s)=\frac{1}{Z_{\rm cable}\left(1+L_fC_fs^2\right)+s\left[L_f+L_l+L_lL_fC_fs^2\right]}\cdot V_{\rm inv}(s)+\frac{-L_fC_fs^2-1}{Z_{\rm cable}\left(1+L_fC_fs^2\right)+s\left[L_f+L_l+L_lL_fC_fs^2\right]}\cdot V_g(s)=G_{V_{\rm inv}\to I_l}(s)\cdot V_{\rm inv}(s)+G_{V_g\to I_l}(s)\cdot V_g(s). \quad (4)$$

Fig. 4 shows the bode diagrams of $G^{\rm old}_{V_{\rm inv}\to I_l}(s)$ and $G_{V_{\rm inv}\to I_l}(s)$ from the two different cable models, respectively. The parameters used in Fig. 4 are listed in Table I. Only one pole (resonance) appeared in $G^{\rm old}_{V_{\rm inv}\to I_l}(s)$, but multipoles would exist in the cascaded π-segments of a cable. It means that more complicated damping strategies are needed for a real cable-based system to damp the resonant peaks below 0 dB. For the case of the *LCL* filter, it is possible to use multiloop damping methods to attenuate the resonance. However, it is difficult to damp the resonances of the real cable due to the unknown current or voltage inside the cable.

III. Proposed Control Strategy

A. System Analysis

In general, the inverter current or the grid (cable) current is used as a feedback for the current controller to regulate the current penetrated into the grid [20]. With the viewpoint of grid current penetration, the conventional current control loop with the grid (cable) current feedback is presented in Fig. 5 to analyze the system stability. The cable current command I_l^* is determined by available renewable (i.e., wind) power. G_C is the current regulator determined by the special control strategy, $G_{\rm inv}$ is the inverter transfer function including the PWM switching delay, and V_g is the grid voltage. The measured cable input current is introduced to the current controller through a feedback proportional gain (H). $G_{V_{\rm inv}\to I_l}(s)$ is the $V-I$ transfer function of the *LCL* filter + Cable configuration, given by (4) for the cable current feedback. Without the consideration of grid voltage distortion, the open-loop transfer function $G_{\rm open}(s)$ then can be expressed as

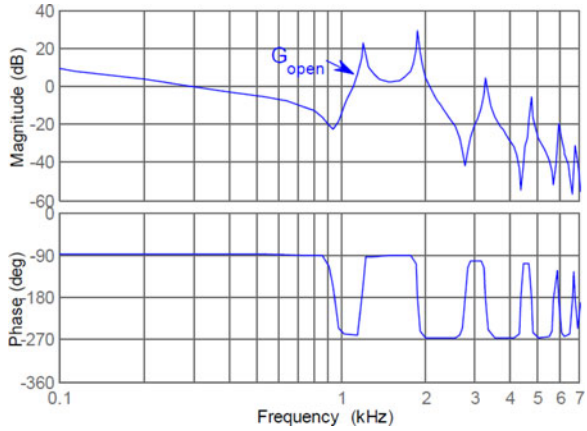

Fig. 6. Bode plot of the open-loop transfer function $G_{\rm open}(s)$.

$$G_{\rm open}(s)=G_C(s)\cdot G_{\rm inv}(s)\cdot G_{V_{\rm inv}\to I_l}(s)\cdot H. \quad (5)$$

The steady-state error can be derived as

$$E(s)=I_l^*-I_l=\frac{I_l^*}{1+G_{\rm open}(s)}. \quad (6)$$

The transfer function of the PWM VSI can be expressed approximately as

$$G_{\rm inv}(s)=V_{\rm DC}e^{-T_ds} \quad (7)$$

where T_d is the PWM control delay.

Fig. 6 shows the bode diagram of the open-loop transfer function $G_{\rm open}(s)$. If a PI regulator is used, then G_C can be described as

$$G_C(s)=K_P\left(1+\frac{K_i}{S}\right). \quad (8)$$

For the purpose of the system stability, the proportional gain K_P is limited due to the peaks existing at the resonant frequencies of $G_{\rm open}(s)$, as illustrated in Fig. 6. Hence, the control loop gain for the traditional strategy is quite small, and the system output is not able to track a sinusoidal reference with zero error. Hence, the PI regulator is impossible to be adapted here to achieve both system stability and reference tracking.

B. Factors to Affect the Resonant Peaks

A series of $G_{\rm open}(s)$ with different system specifications, i.e., different filter parameters and transformer leakage inductances, will be analyzed in order to clearly understand the essential influences caused by the cable impedance.

1) Filter Parameters Influence on $G_{\rm open}(s)$: The general requirements of a filter (i.e., *LC* type) design are as follows: 1) to have a cutoff frequency lower than the switching frequency of

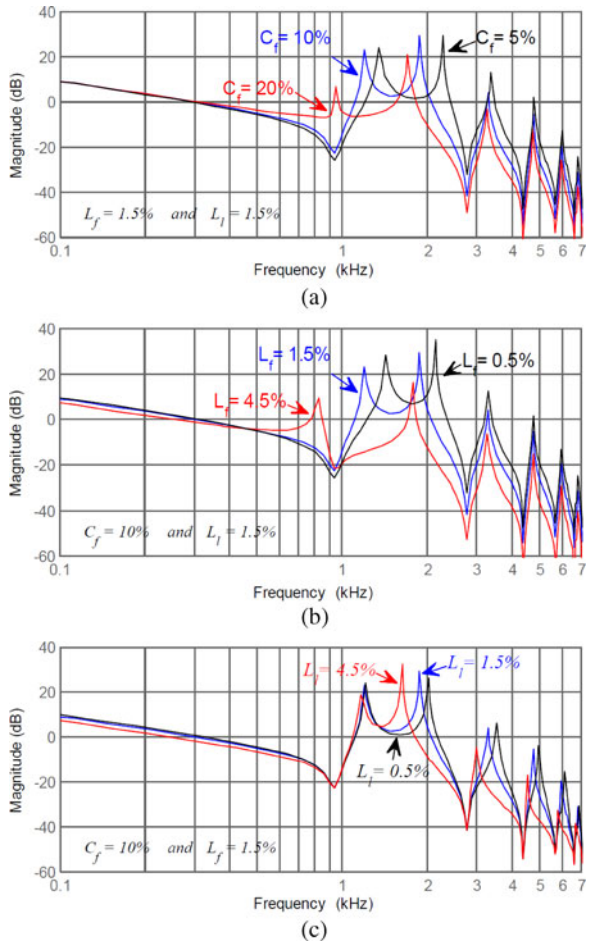

Fig. 7. Bode plots of $G_{\rm open}$ with different system parameters. (a) Different filter capacitances. (b) Different filter inductances. (c) Different transformer leakage inductances.

the converter; 2) to minimize its reactive power under the rated condition; and 3) to minimize the filter inductance voltage drop at the rated current in order to avoid a reduction in a voltage transfer ratio. According to these guidelines, the reactive power of the filter usually should be limited to less than 5–10% of the rated power in order to ensure high power factor.

The bode diagram of $G_{\rm open}(s)$ with different filter capacitances is shown in Fig. 7(a) in order to evaluate the filter capacitance's influence on $G_{\rm open}(s)$. Herein, the system parameters are listed in Table I. From Fig. 7(a), the resonance peaks on the high-frequency domain would be increased along with the decrease of the capacitance. A large filter capacitance provides a limited attenuation on the first and second resonant peaks although it presents an effective attenuation on the high-frequency resonant peaks. Most importantly, the large capacitance would draw from or supply much reactive current, which, in turn, worse the inverter power factor. Hence, a compromise is made in this study to select the capacitance as 10%.

Traditionally, the filter inductance is designed by the cutoff frequency f_C, which should be lower by 1/20th to 1/10th of the switching frequency f_S. Fig. 7(b) illustrates the bode plots of $G_{\rm open}(s)$ under different filter inductances. It can be seen that the large inductance has an attenuation on the resonant peaks in some extents; however, the resonant peaks will not be eliminated by the inductance, especially on the first and second resonant peaks. Hence, the inductance is then set as 1.5% based on the practical design principle of a filter.

2) Transformer Leakage Inductance Influence on $G_{\rm open}(s)$: For a distribution-level transformer, the leakage inductance of the transformer is in a range of 1–15%, which is determined by the system/grid operator requirement [44]. The transformer leakage inductance is relative small in reliable systems with aims to reduce reactive power consumption. Herein, in order to evaluate the leakage inductance influence on $G_{\rm open}(s)$, the bode plots of $G_{\rm open}(s)$ with different leakage inductances are shown in Fig. 7(c). It can be found that the leakage inductances have similar influence on $G_{\rm open}(s)$ as that of the filter capacitance. The high-frequency attenuation is more and more obvious by the increase of the transformer leakage inductance. However, the low resonant peaks are not attenuated effectively. To sum up, the filter parameters and the leakage inductances would not affect the low-frequency resonances as effectively as the high-frequency resonant peaks. Hence, in order to eliminate the low-frequency resonant peaks, it is required to design an effective damping controller.

C. Proposed Control Strategy

As aforesaid, it is possible to make the system stable by drastically reducing the proportional gain of the PI controller. However, this yields poor bandwidth and disturbance rejection capability; hence, it will not be considered here. The requirement of the potential control strategies is to obtain resonance damping while preserving reasonable bandwidth as well as stability and robustness margins.

To achieve this target, filter-based damping strategies will be explored to address the resonance peaks of the system open-loop transfer function $G_{\rm open}(s)$, as shown in Fig. 6. The performance/effectiveness of filter-based damping techniques will be evaluated by the following two criteria: the first one is to attenuate the resonance peak of the gain response. However, as the resonance peak is very high, a rather sharp filter characteristic is required. Otherwise, the closed-loop bandwidth is decreased considerably. On the other hand, it is required to avoid -180° crossings in the frequency range with a gain above 0 dB. Note that the gain and phase responses cannot be modified separately.

With the aforementioned theoretical analysis, a notch filter is employed to damp the gain resonance because of its stop-band filter characteristic. The continuous transfer function of the standard notch filter can be expressed as

$$G_{{\rm notch},i} = \frac{s^2 + \omega_i^2}{s^2 + bs + \omega_i^2} \tag{9}$$

where ω_i is the notch frequency where signal can be mostly attenuated by the filter and b is the filter bandwidth. The deepness and wideness of the notch filter will be decided by the damping of the zeros and of the poles of the filter, respectively. Actually, the notch filter is often used to filter out the undesired signal in the specific frequency only. Fig. 8(a) shows the bode plot of the

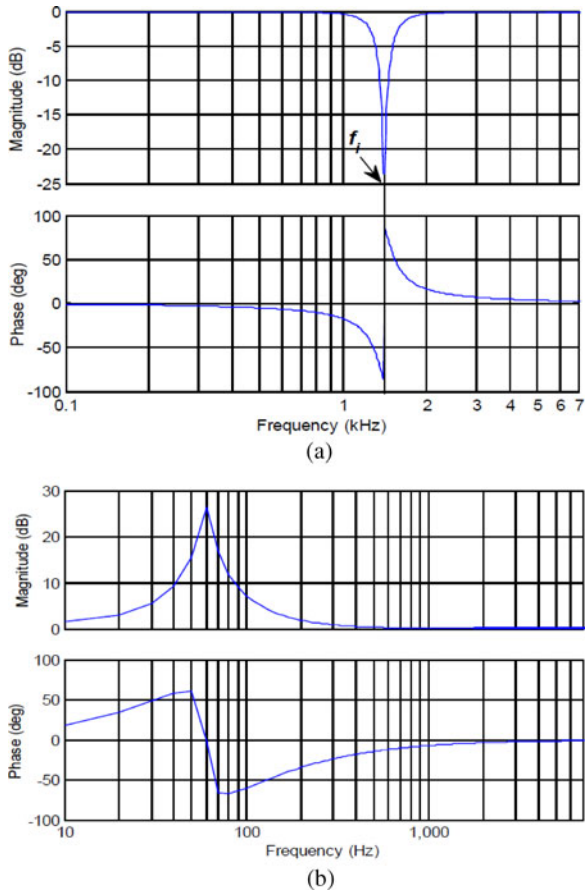

Fig. 8. Bode plots of the notch filter and the PR controller. (a) Notch filter. (b) PR controller.

notch filter. It has a V-shaped magnitude characteristic, with the gain remaining fairly close to unity up to the neighborhood of the notch point, and then falling off abruptly with a descending rate much greater than that of a second-order filter [45]. This behavior is suitable for canceling out the resonant peak without appreciable attenuation at lower frequencies.

Again, from Fig. 6, the multiple resonant frequencies exist with the consideration of the cable characteristic. The notch filters are used to attenuate multiple resonance peaks; as a sequence, the so-called cascaded notch-filter (multiple notch filters in series) is proposed to damp the significant resonance peaks. The order of the cascaded notch filter is determined by the number of peaks, of which the magnitude is above 0 dB.

On the other hand, a PR controller is able to provide high gain at the fundamental frequency and thus reduces the steady-state error [46]–[48]. The expression of a PR controller is as follows:

$$G_{\mathrm{PR}} = K_P + \frac{2K_C(\omega_C s + \omega_C^2)}{s^2 + 2\omega_C s + (\omega_0^2 + \omega_C^2)} \tag{10}$$

where ω_C is the equivalent bandwidth of the controller, K_P and K_C are the proportional and resonant gain, respectively, and ω_0 is the frequency that needs a high gain on it. ω_C needs to be set as small as possible because a large ω_C will introduce a phase lag toward the crossover frequency and thus decreases the phase margin. Fig. 8(b) shows the bode plots of the PR controller.

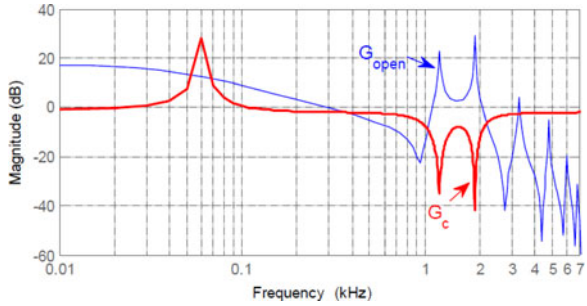

Fig. 9. Bode diagram of the proposed controller.

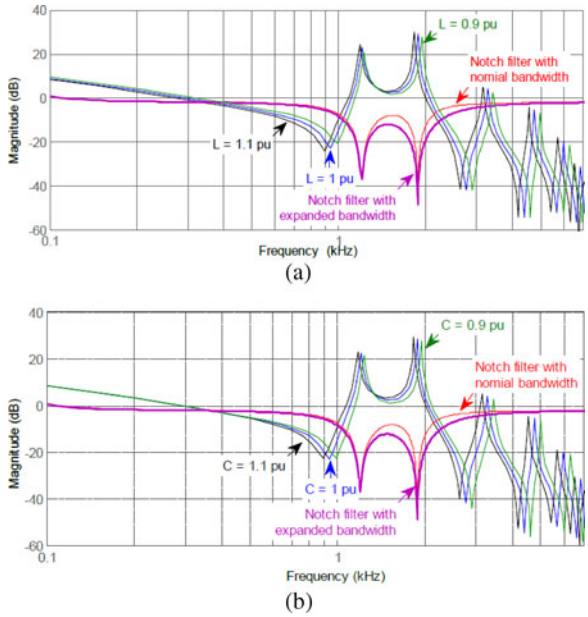

Fig. 10. Bode diagram of the proposed controller with the cable parameter fluctuation. (a) Different cable inductances per length. (b) Different cable capacitances per length.

With the previous analysis, the proposed controller G_C can be expressed as

$$G_C = G_{\mathrm{PR}} \cdot \prod_{i=1}^{n} G_{\mathrm{notch},i} \tag{11}$$

where n is the order of the cascaded notch filter. For the case in Fig. 6, two cascaded notch filters are sufficient to damp the resonance peaks. Fig. 9 shows the bode plots of the proposed controller, which is used to damp the resonances existed in the system.

D. Parameter Selection of the Notch Filters

To achieve the best damping performance, the center frequency of the notch filter is desired to exactly match with the cable resonant peaks since the notch filter is often used to filter out the undesired signal in the specific frequency only. However, it is a challenge to calculate the resonant frequencies accurately due to the fluctuation of the cable parameters. Fig. 10(a) and (b) shows the resonant frequencies versus the fluctuation of the cable inductance and capacitance, respectively. The system

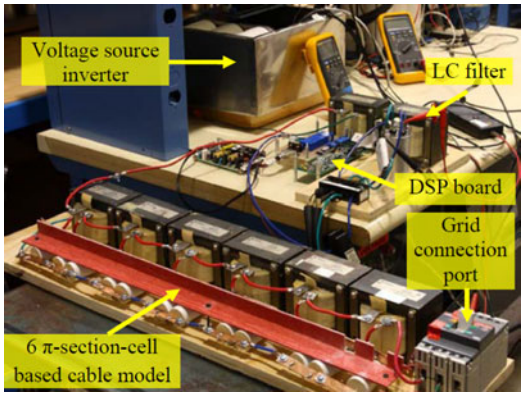

Fig. 11. Photograph of the experimental setup.

specification is listed in Table I. It can be found that the resonant frequencies tend to deviate from the rated resonant peaks, which would degrade the damping performance of the developed method.

To address this challenge, the bandwidth of the notch filter needs to be expanded in order to make the notch filter insensitive to the fluctuation of the resonances within a given range. The purpose is to attenuate the system resonant peaks under 0 dB with the notch filters and thereby guarantee the system stability. It is worthy to point out that the significant increase of the notch filter bandwidth would potentially reduce the system phase margin, and hence, there is a tradeoff during the design of the notch filter. In practice, the bandwidth b of the notch filter as shown in (9) can be adjusted accordingly as illustrated in Fig. 10, which, in turn, addresses the potential fluctuation of the system resonant peaks.

IV. Simulation and Experimental Verification

The simulation and experimental verifications of the proposed control scheme will be carried out on a per-unit scale emulator in a laboratory. The offshore wind farm emulator is composed of a full-bridge single-phase inverter, an *LC* filter, a line inductor, a lumped *LC* network with 6 π-section cells, and a 120 V_{ac} grid, as shown in Fig. 11. A digital signal processor TMS320F28035 is used to control the single-phase inverter. From the Nyquist law, the controller's sampling frequency should be higher than twice the resonance frequencies in order to actively compensate the high-frequency resonance poles. Hence, the sampling frequency of the output voltage and the PWM switching frequency are both of 10 kHz. The inverter was designed to operate in a 200 V_{dc} bus. The detailed specifications are listed in Table I.

A high-voltage high-power system is always represented by a low-voltage low-power system with the same per-unit value for the convenience of theoretical analysis [49]. The per-unit length parameters of the cable from the Horn Rev wind farm are multiplied with the distance, which corresponds to the 1/6th of the entire cable length with the 6 π-section-cell-based model. We can then calculate the inductance and capacitance of each cell, which is used to build the per-unit scale laboratory demonstrator. Hence, the laboratory demonstrator would have the same

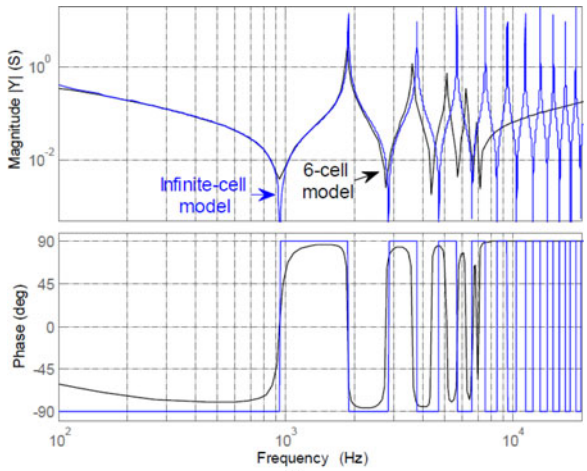

(a)

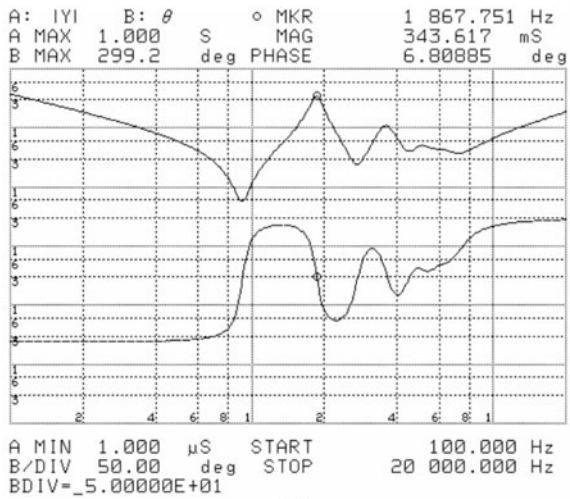

(b)

Fig. 12. Transmission cable admittance. (a) Infinite π-cell and 6 π-cell model. (b) Experimental measurement of the six-cell model.

resonant frequencies as the real wind farm in the case of the same per-unit length parameters and the same cable length.

In addition, the selection criteria of the 6 π-section-cell-based cable model are as follows. The resonant peaks, which need to be damped, are all less than 3 kHz from the previous analysis in Section III. Therefore, the frequencies less than 3 kHz are our focused range. Thus, the total cable length is of 42 km from the Horn Rev wind farm, which is divided into six segments. The length of each segment is then 7 km, which is less than one-tenth of the wavelength at the frequency of interest ($<$3 kHz). On the other hand, from the viewpoint of practical implementation, it is much flexible to use the 6 π-section-cell-based cable model rather than the theoretical cable model with an infinite π-section cell. The comparison of their bode diagrams is presented in Fig. 12(a). It can be found that the 6 π-section cell-based model is matched well with the theoretical model in the first several resonant peaks. As discussed previously, only the low-frequency resonant peaks are required to be damped because the high-frequency resonant peaks have been attenuated significantly by the resistance. Hence, the 6 π-section-cell-based

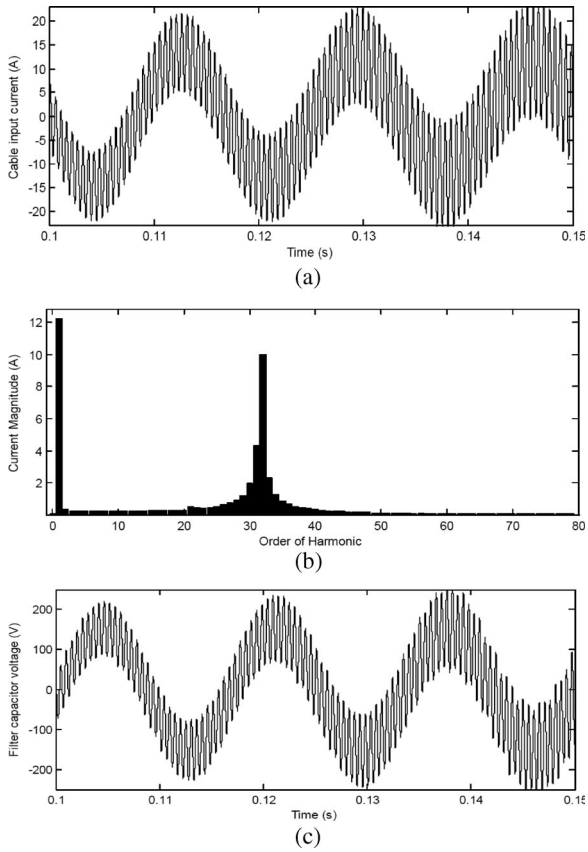

Fig. 13. Simulation waveforms of the cable current and filter capacitor voltage with the PR controller only.

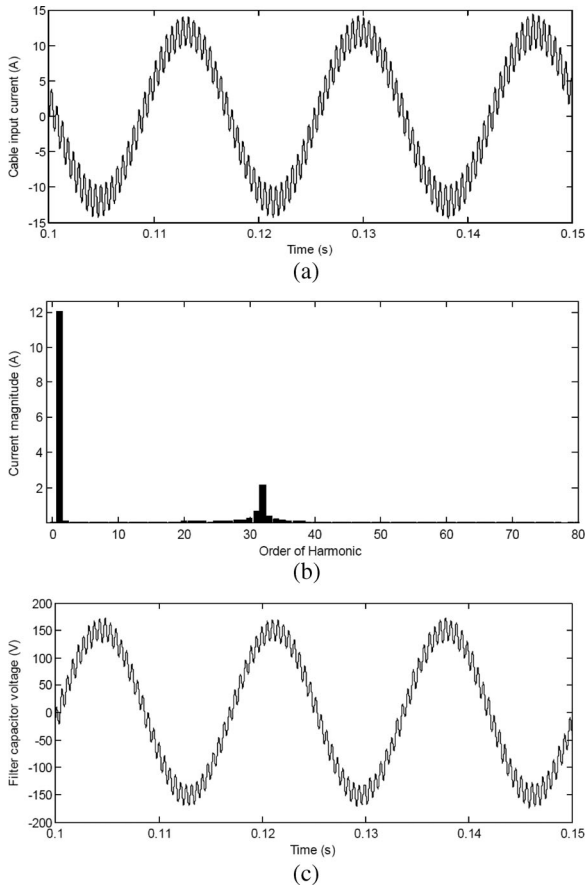

Fig. 14. Simulation waveforms of the cable current and the filter capacitor voltage when using PR and one notch filter with center frequency at 1.2 kHz.

model is accurate enough to exhibit the lower frequency resonances. An HP 4194 impedance analyzer is used to measure the characteristic of the 6 π-section-cell-based cable model, which is illustrated in Fig. 12(b). It further demonstrates the accuracy of the built cable model.

A. Simulation Results

The control loop gain for the traditional strategy (the PI controller) is quite small to ensure the system's stability, and thereby, the steady-state error of the system output will be significant. To overcome this disadvantage, the PR controller is used to replace the PI controller to reduce the steady-state error. Fig. 13 shows the simulation results of the filter capacitor voltage, the input current of the cable, and its spectrum analysis with the PR controller only. The system would be unstable due to the resonant peaks of $G_{\mathrm{open}}(s)$, as shown in Fig. 6. From the current spectrum analysis, it can be found that a series of resonant frequencies is existed from around 1.2 to 2 kHz, which is identical to the aforementioned theoretical analysis. As a result, there are significant resonances in both the cable current and the filter capacitor voltage, and thereby cause system unstable. Hence, the conventional system would encounter the challenge of system stability due to the transmission cable's characteristics.

With the proposed strategy, the cascaded notch filter is adapted to compensate the resonant peaks caused by the system setup. In the case of one notch filter with a centered frequency of 1.2 kHz, the compensated results of the capacitor voltage, the cable current, and its spectrum analysis are illustrated in Fig. 14. To some extent, the resonant phenomenon can be relieved by the notch filter since one of the resonant peak can be attenuated. However, another significant peak is still at 1.8 kHz.

Fig. 15 shows the simulation results of the capacitor voltage, and the cable current when the PR and two notch filters (1.2 and 1.8 kHz) are employed. The resonant phenomenon has been completely attenuated, which is identical to the theoretical analysis.

B. Experimental Results

Fig. 16 shows the experimental results of the capacitor voltage, the cable input current, and its spectrum analysis with the PR controller only. The resonance phenomenon is obvious in the voltage and current. During the experiment, the controller gain is limited at 5 dB in order to relieve the resonance, which, in turn, protects the front-end inverter. Without the notch filters, the most severe resonance occurs at around 1.6 kHz, which exactly stands for the unstable poles in the closed-loop system.

To damp the resonant peaks caused by the cable, a notch filter with the center frequency at 1.2 kHz is cascaded with the PR controller and then the experimental results are shown in Fig. 17. It can be seen that the resonance frequency is shifted

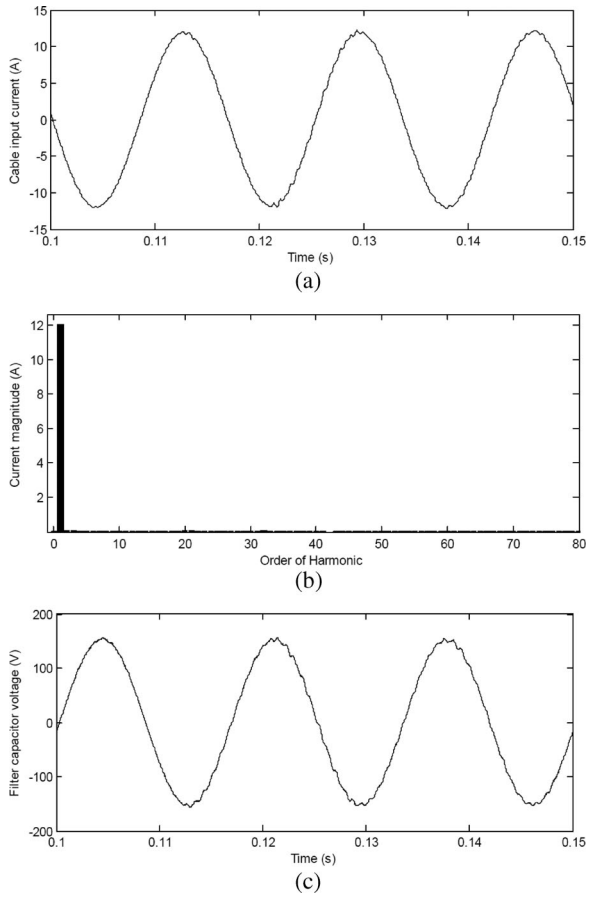

Fig. 15. Simulation waveforms of the cable current and the filter capacitor voltage when using PR and two notch filters.

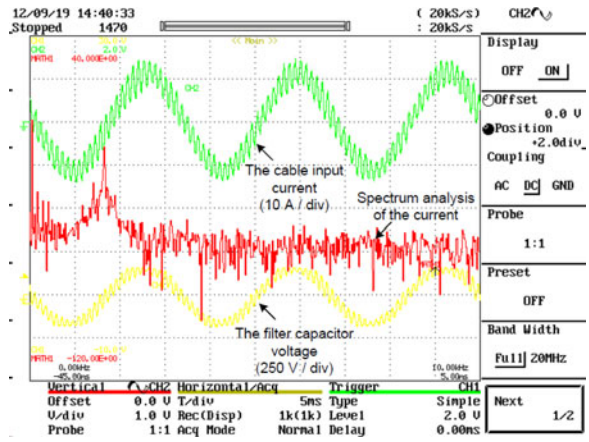

Fig. 16. Experimental waveforms of the cable current and the filter capacitor voltage with the PR controller only.

to around 1.8 kHz. It is identical to the theoretical analysis and simulation.

To further damp the resonant peak at 1.8 kHz, another notch filter with the center frequency at 1.8 kHz is involved into the controller, and thereby, two notch filters are cascaded with the PR controller. Fig. 18 shows the experimental results of the

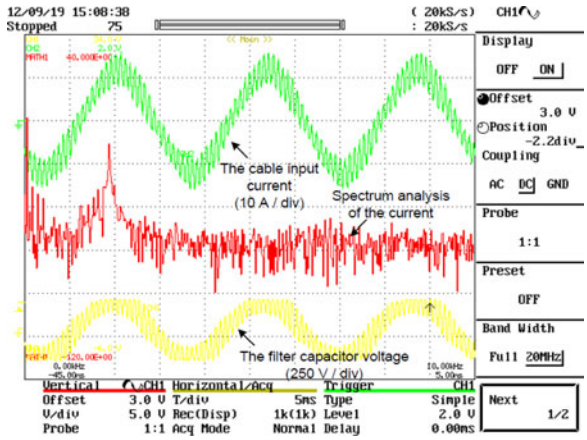

Fig. 17. Experimental waveforms of the cable current and the filter capacitor voltage when using PR and one notch filter.

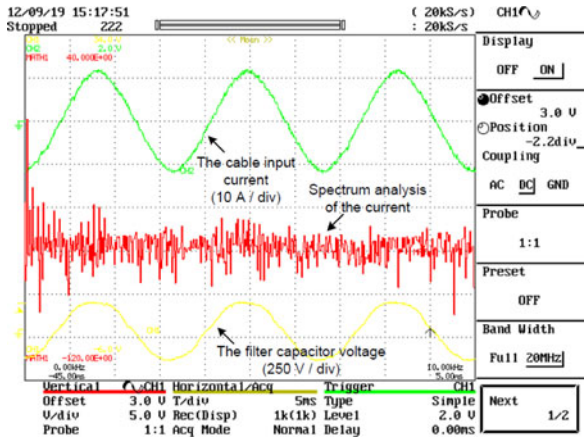

Fig. 18. Experimental waveforms of the cable current and the filter capacitor voltage when using PR and two notch filters.

voltage and current. In this case, the first two resonance peaks depicted in Fig. 6 are well attenuated, and the closed-loop system is then stabilized. A THD of 2.34% is achieved in the output current.

Fig. 19 shows the dynamic response of the whole system. The current references in Fig. 19(a) and (b) have a step change from 4 to 8 A and then from 8 to 4 A, respectively. It can be seen that the proposed controller can effectively damp the system resonance, which, in turn, makes system stable. Moreover, a fast transient response is also achieved by the proposed control strategy.

V. Conclusion

The grid-connected offshore wind farms consist of wind turbine generators, voltage source converters, step-up transformers, and submarine cables. The high shunt capacitance of the submarine cable can cause severe high-frequency resonance. This paper disclosed this phenomenon and developed the per-unit scale single-phase equivalent model of the HVac-connected wind generation system. Due to the high-order *LC* configuration, the system open-loop transfer function exhibited a series of significant high-frequency resonant peaks, which

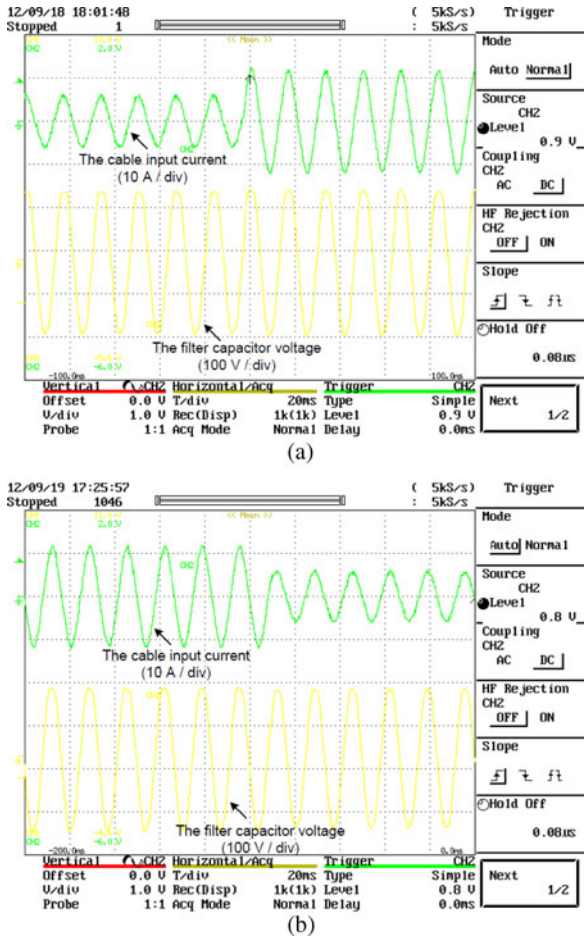

Fig. 19. Experimental results of the dynamic performance of the proposed control strategy. (a) Cable current reference step-up. (b) Cable current reference step-down.

makes system unstable. Frequency-domain analysis has been carried out to identify the key passive components that have a significant impact on the system high-frequency characteristics rather than the lower frequency feature. The cascaded notch-filter-based active damping method was proposed to overcome the lower frequency resonances, which, in turn, guarantee system stability. Furthermore, the proposed controller consisted of the PR component reduced steady-state error of the system output. The simulation and experimental results have demonstrated the findings of resonances and the performance of the proposed controller.

REFERENCES

[1] J. M. Carrasco, L. G. Franquelo, J. T. Bialasiewicz, E. Galvan, R. C. P. Guisado, Ma A. M. Prats, J. I. Leon, and N. Moreno-Alfonso, "Power-electronic systems for the grid integration of renewable energy sources: A Survey," *IEEE Trans. Ind. Electron.*, vol. 53, no. 4, pp. 1002–1016, Jun. 2006.

[2] S. B. Kjaer, J. K. Pedersen, and F. Blaabjerg, "A review of single-phase grid-connected inverters for photovoltaic modules," *IEEE Trans. Ind. Appl.*, vol. 41, no. 5, pp. 1292–1306, Sep./Oct. 2005.

[3] N. Flourentzou, V. G. Agelidis, and G. D. Demetriades, "VSC-based HVDC power transmission systems: An overview," *IEEE Trans. Power Electron.*, vol. 24, no. 3, pp. 592–602, Mar. 2009.

[4] M. Chinchilla, S. Arnaltes, and J. C. Burgos, "Control of permanent-magnet generators applied to variable-speed wind-energy systems connected to the grid," *IEEE Trans. Energy Convers.*, vol. 21, no. 1, pp. 130–135, Mar. 2006.

[5] P. Bresesti, W. L. Kling, R. L. Hendriks, and R. Vailati, "HVDC connection of offshore wind farms to the transmission system," *IEEE Trans. Energy Convers.*, vol. 22, no. 1, pp. 37–43, Mar. 2007.

[6] F. Blaabjerg, R. Teodorescu, M. Liserre, and A. V. Timbus, "Overview of control and grid synchronization for distributed power generation systems," *IEEE Trans. Ind. Electron.*, vol. 53, no. 5, pp. 1398–1409, Oct. 2006.

[7] L. P. Chiang and D. G. Holmes, "Analysis of multiloop control strategies for LC/CL/LCL-filtered voltage-source and current-source inverters," *IEEE Trans. Ind. Appl.*, vol. 41, no. 2, pp. 644–654, Mar./Apr. 2005.

[8] Wu Weimin, He Yuanbin, and F. Blaabjerg, "An LLCL power filter for single-phase grid-tied inverter," *IEEE Trans. Power Electron.*, vol. 27, no. 2, pp. 782–789, Feb. 2012.

[9] J. Muhlethaler, M. Schweizer, R. Blattmann, J. W. Kolar, and A. Ecklebe, "Optimal design of LCL harmonic filters for three-phase PFC rectifiers," *IEEE Trans. Power Electron.*, vol. 28, no. 7, pp. 3114–3125, Jul. 2013.

[10] M. Liserre, F. Blaabjerg, and R. Teodorescu, "Grid impedance estimation via excitation of LCL-filter resonance," *IEEE Trans. Ind. Appl.*, vol. 43, no. 5, pp. 1401–1407, Sep./Oct. 2007.

[11] I. J. Gabe, V. F. Montagner, and H. Pinheiro, "Design and implementation of a robust current controller for VSI connected to the grid through an LCL filter," *IEEE Trans. Power Electron.*, vol. 24, no. 6, pp. 1444–1452, Jun. 2009.

[12] S. Zhang, K.-J. Tseng, M. M. Vilathgamuwa, T. D. Nguyen, and X.-Y. Wang, "Design of a robust grid interface system for PMSG-Based wind turbine generators," *IEEE Trans. Ind. Electron.*, vol. 58, no. 1, pp. 316–328, Jan. 2011.

[13] Twining Erika and D. G. Holmes, "Grid current regulation of a three-phase voltage source inverter with an LCL input filter," *IEEE Trans. Power Electron.*, vol. 18, no. 3, pp. 888–895, May 2003.

[14] M. Liserre, A. Dell'Aquila, and F. Blaabjerg, "Genetic algorithm-based design of the active damping for an LCL-filter three-phase active rectifier," *IEEE Trans. Power Electron.*, vol. 19, no. 1, pp. 76–86, Jan. 2004.

[15] J. Dannehl, C. Wessels, and F. W. Fuchs, "Limitations of voltage-oriented PI current control of grid-connected PWM rectifiers with LCL filters," *IEEE Trans. Ind. Electron.*, vol. 56, no. 2, pp. 380–388, Feb. 2009.

[16] B. Bolsens, K. De Brabandere, J. Van den Keybus, J. Driesen, and R. Belmans, "Model-based generation of low distortion currents in grid-coupled PWM-inverters using an LCL output filter," *IEEE Trans. Power Electron.*, vol. 21, no. 4, pp. 1032–1040, Jul. 2006.

[17] T. Abeyasekera, C. M. Johnson, D. J. Atkinson, and M. Armstrong, "Suppression of line voltage related distortion in current controlled grid connected inverters," *IEEE Trans. Power Electron.*, vol. 20, no. 6, pp. 1393–1401, Nov. 2005.

[18] M. Liserre, F. Blaabjerg, and S. Hansen, "Design and control of an LCL-filter-based three-phase active rectifier," *IEEE Trans. Ind. Appl.*, vol. 41, no. 5, pp. 1281–1291, Sep./Oct. 2005.

[19] R. Pena-Alzola, M. Liserre, F. Blaabjerg, R. Sebastian, J. Dannehl, and F. W. Fuchs, "Analysis of the passive damping losses in LCL-filter-based grid converters," *IEEE Trans. Power Electron.*, vol. 28, no. 6, pp. 2642–2646, Jun. 2013.

[20] Shen Guoqiao, Xu Dehong, Cao Luping, and Zhu Xuancai, "An improved control strategy for grid-connected voltage source inverters with an LCL filter," *IEEE Trans. Power Electron.*, vol. 23, no. 4, pp. 1899–1906, Jul. 2008.

[21] J. Dannehl, F. W. Fuchs, S. Hansen, and P. B. Thøgersen, "Investigation of active damping approaches for PI-Based current control of grid-connected pulse width modulation converters with LCL filters," *IEEE Trans. Ind. Appl.*, vol. 46, no. 4, pp. 1509–1517, Jul./Aug. 2010.

[22] Y. W. Li, "Control and resonance damping of voltage-source and current-source converters with LC filters," *IEEE Trans. Ind. Electron.*, vol. 56, no. 5, pp. 1511–1521, May 2009.

[23] M. Liserre, R. Teodorescu, and F. Blaabjerg, "Stability of photovoltaic and wind turbine grid-connected inverters for a large set of grid impedance values," *IEEE Trans. Power Electron.*, vol. 21, no. 1, pp. 263–272, Jan. 2006.

[24] F. Liu, Y. Zhou, S. Duan, J. Yin, B. Liu, and F. Liu, "Parameter design of a two-current-loop controller used in a grid-connected inverter system with LCL filter," *IEEE Trans. Ind. Electron.*, vol. 56, no. 11, pp. 4483–4491, Nov. 2009.

[25] S. Mariethoz and M. Morari, "Explicit model-predictive control of a PWM inverter with an LCL filter," *IEEE Trans. Ind. Electron.*, vol. 56, no. 2, pp. 389–399, Feb. 2009.
[26] J. L. Agorreta, M. Borrega, J. Lopez, and L. Marroyo, "Modeling and control of N-paralleled grid-connected inverters with LCL filter coupled due to grid impedance in PV plants," *IEEE Trans. Power Electron.*, vol. 26, no. 3, pp. 770–785, Mar. 2011.
[27] X. Wang, X.-B. Ruan, S. Liu, and C. K. Tse, "Full feedforward of grid voltage for grid-connected inverter with LCL filter to suppress current distortion due to grid voltage harmonics," *IEEE Trans. Power Electron.*, vol. 25, no. 12, pp. 3119–3127, Dec. 2010.
[28] J. Dannehl, M. Liserre, and F. W. Fuchs, "Filter-based active damping of voltage source converters with LCL filter," *IEEE Trans. Ind. Electron.*, vol. 58, no. 8, pp. 3623–3633, Aug. 2011.
[29] L. A. Serpa, S. Ponnaluri, P. M. Barbosa, and J. W. Kolar, "A modified direct power control strategy allowing the connection of three-phase inverters to the grid through LCL filters," *IEEE Trans. Ind. Appl.*, vol. 43, no. 5, pp. 1388–1400, Sep./Oct. 2007.
[30] E. Wu and P. W. Lehn, "Digital current control of a voltage source converter with active damping of LCL resonance," *IEEE Trans. Power Electron.*, vol. 21, no. 5, pp. 1364–1373, Sep. 2006.
[31] J. R. Massing, M. Stefanello, H. A. Grundling, and H. Pinheiro, "Adaptive current control for grid-connected converters with LCL filter," *IEEE Trans. Ind. Electron.*, vol. 59, no. 12, pp. 4681–4693, Dec. 2012.
[32] J. He and Y. W. Li, "Generalized closed-loop control schemes with embedded virtual impedances for voltage source converters with LC or LCL filters," *IEEE Trans. Power Electron.*, vol. 27, no. 4, pp. 1850–1861, Apr. 2012.
[33] M. Malinowski and S. Bernet, "A simple voltage sensorless active damping scheme for three-phase PWM converters with an LCL filter," *IEEE Trans. Ind. Electron.*, vol. 55, no. 4, pp. 1876–1880, Apr. 2008.
[34] C. J. Chou, Y. K. Wu, G. Y. Han, and C. Y. Lee, "Comparative evaluation of the HVDC and HVAC links integrated in a large offshore wind farm: An actual case study in Taiwan," *IEEE Trans. Ind. Appl.*, vol. 48, no. 5, pp. 1639–1648, Sep./Oct. 2012.
[35] J. W. Phinney, D. J. Perreault, and J. H. Lang, "Synthesis of lumped transmission-line analogs," *IEEE Trans. Power Electron.*, vol. 22, no. 4, pp. 1531–1542, Jul. 2007.
[36] L. Paulsson, B. Ekehov, S. Halen, T. Larsson, L. Palmqvist, A. A. Edris, D. Kidd, A. J. F. Keri, and B. Mehraban, "High-frequency impacts in a converter-based back-to-back tie; the Eagle Pass installation," *IEEE Trans. Power Del.*, vol. 18, no. 4, pp. 1410–1415, Oct. 2003.
[37] A. Pagnetti, A. Xemard, F. Paladian, and C. A. Nucci, "An improved method for the calculation of the internal impedances of solid and hollow conductors with the inclusion of proximity effect," *IEEE Trans. Power Del.*, vol. 27, no. 4, pp. 2063–2072, Oct. 2012.
[38] C. H Chien and R. Bucknall, "Harmonic calculations of proximity effect on impedance characteristics in Subsea power transmission cables," *IEEE Trans. Power Del.*, vol. 24, no. 4, pp. 2150–2158, Oct. 2009.
[39] B. Badrzadeh, M. Hogdahl, and E. Isabegovic, "Transients in wind power plants: Part I. Modeling methodology and validation," *IEEE Trans. Ind. Appl.*, vol. 48, no. 2, pp. 794–807, Mar./Apr. 2012.
[40] R. K. Varma, S. Auddy, and Y. Semsedini, "Mitigation of subsynchronous resonance in a series-compensated wind farm using FACTS controllers," *IEEE Trans. Power Del.*, vol. 23, no. 3, pp. 1645–1654, Jul. 2008.
[41] Zhang Shao, Tseng King-Jet, Choi San Shing, Nguyen Trong Duy, and Yao Dai Lin, "Advanced control of series voltage compensation to enhance wind turbine ride through," *IEEE Trans. Power Electron.*, vol. 27, no. 2, pp. 763–772, Feb. 2012.
[42] C.-S. Yen, Z. Fazarinc, and R. L. Wheeler, "Time-domain skin-effect model for transient analysis of lossy transmission lines," *Proc. IEEE*, vol. 70, no. 7, pp. 750–757, 1982.
[43] Thomas H. Lee, *The Design of CMOS Radio-Frequency Integrated Circuits*, 2nd ed. Cambridge, U.K.: Cambridge Univ. Press, 2004.
[44] J. C. Das, *Power System Analysis: Short-Circuit Load Flow and Harmonics*. New York, NY, USA: Marcel Dekker, 2002.
[45] K. Zhang, Y. Kang, J. Xiong, and J. Chen, "Direct repetitive control of SPWM inverter for UPS purpose," *IEEE Trans. Power Electron.*, vol. 18, no. 3, pp. 784–792, May 2003.
[46] D. G. Holmes, T. A. Lipo, B. P. McGrath, and W. Y. Kong, "Optimized design of stationary frame three phase AC current regulators," *IEEE Trans. Power Electron.*, vol. 24, no. 11, pp. 2417–2426, Nov. 2009.
[47] M. Liserre, R. Teodorescu, and F. Blaabjerg, "Multiple harmonics control for three-phase grid converter systems with the use of PI-RES current controller in a rotating frame," *IEEE Trans. Power Electron.*, vol. 21, no. 3, pp. 836–841, May 2006.
[48] R. Teodorescu, F. Blaabjerg, M. Liserre, and P. C. Loh, "Proportional-resonant controllers and filters for grid-connected voltage-source converters," *IEE Proc.—Elect. Power Appl.*, vol. 153, no. 5, pp. 750–762, Sep. 2006.
[49] W. D. Stevenson, *Elements of Power System Analysis*, 4th ed. New York, NY, USA: McGraw-Hill, 1982.

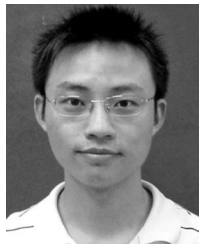

Shao Zhang (S'09–M'13) received the B.Sc. and M.Sc. degrees in electrical engineering from Nanjing University of Aeronautics and Astronautics, Nanjing, China, in 2003 and 2006, respectively, and the Ph.D. degree from Nanyang Technological University, Singapore, in 2011.

He is now a Research Scholar in Michigan State University, East Lansing, MI, USA. His current research interests include power electronic converters, electrical drives, renewable energy integration with grids, and energy storage.

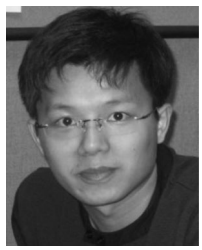

Shuai Jiang (S'11) received the B.S. degree in electronics and information engineering from Shanghai Jiao Tong University, Shanghai, China, in 2005. He is currently working toward the Ph.D. degree at Michigan State University, East Lansing, MI,USA.

From 2005 to 2009, he was with Schneider Electric as an Electronics Design Engineer, and was involved in the development of power meters, circuit monitors, and wireless switches. His research interests include Z-source inverters, UPS, and grid-connected inverters.

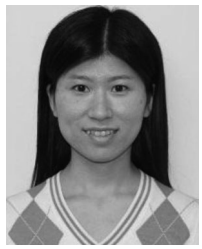

Xi Lu (S'09) received the B.S. degree from Huazhong University of Science and Technology, Wuhan, China, in 2007. From 2007 to 2013, she has been working toward the M.S. and Ph.D. degrees at Michigan State University, East Lansing, MI, USA.

Since 2013, she has been with Ford Motor Company as a Power Electronics Research Engineer.

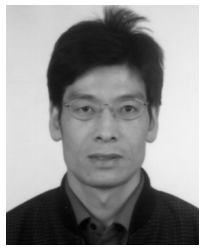

Baoming Ge (M'11) received the Ph.D. Degree in electrical engineering from Zhejiang University, Hangzhou, China, in 2000.

He is currently with Michigan State University; he is also a Professor with Beijing Jiaotong University, Beijing, China. His research interests include PV power generation and wind power generation, permanent magnet synchronous, switched reluctance and induction motors.

Fang Zheng Peng (M'92–SM'96–F'05) received the B.S. degree in electrical engineering from Wuhan University, Wuhan, Hubei, China, in 1983, and the M.S. and Ph.D. degrees in electrical engineering from Nagaoka University of Technology, Nagaoka, Japan, in 1987 and 1990, respectively.

In 2000, he joined Michigan State University, East Lansing, MI, USA, as an Associate Professor and is currently a Full Professor.